LA-UR -81-1453

MASTER

TITLE: THE LOS ALAMOS SYNCHRONOUS ORBIT DATA SET

AUTHOR(S): D. N. Baker, P. R. Higbie, R. D. Belian, E. W. Hones, and R. W. Klebesadel

SUBMITTED TO: Proceedings of the IMS Assessment Symposium
Goddard Space Flight Center, 21-23 May 1981



University of California

LOS ALAMOS SCIENTIFIC LABORATORY
Post Office Box 1663 Los Alamos, New Mexico 87545
An Affirmative Action Equal Opportunity Employer

ABSTRACT

Energetic electron (30-15000 keV) and proton (145 keV - 150 MeV) measurements made by Los Alamos National Laboratory sensors at geostationary orbit (6.6 $R_E$) are summarized. The instrumentation employed and the satellite positions are described. The spacecraft have been variously located, but in their present configuration the Los Alamos satellites designated 1976-059, 1977-007, and 1979-053 are located, respectively, at ~70°W, ~70°E, and ~135°W longitude. Several examples of the high temporal and full three-dimensional spatial measurement capabilities of these instruments are illustrated by examples from the published literature. Discussion is also given for the Los Alamos Synoptic Data Set (SDS) which gives a broad overview of the Los Alamos geostationary orbit measurements. The SDS data are plotted in terms of daily average spectra, 3-hour local time averages, and in a variety of statistical formats. The data summarize conditions from mid-1976 through 1978 (S/C 1976-059) and from early 1977 through 1978 (S/C 1977-007). The SDS compilations presented correspond to measurements at 35°W, 70°W, and 135°W geographic longitude and thus are indicative of conditions at 9°, 11°, and 4.9° geomagnetic latitude, respectively. The bulk of the SDS report presents data plots which are organized according to Carrington solar rotations and, as such, the data are readily comparable to solar rotation-dependent interplanetary conditions. Potential applications of the Synoptic Data Set (available to all interested users in June 1981) are discussed.

## Introduction

The geostationary orbit is a region of considerable human activity in space. At this location, 6.6 $R_E$ (42000 km) from the center of the earth, a spacecraft appears to remain fixed above a given point on the earth's geographic equator since the orbiting satellite completes one revolution as the earth turns once each day. This geostationary orbit is therefore very useful for many satellite applications to weather, communication, and military needs where it is desirable for a spacecraft to maintain a constant position relative to particular geographic locations or land masses.

Scientifically, 6.6 $R_E$ is also a very interesting position within the terrestrial magnetosphere. The geostationary orbit is at the outer terminus of the terrestrial trapped radiation region (outer radiation zone) and is also at the inner edge of the magnetotail plasma sheet. From a geostationary spacecraft platform, therefore, scientific instrumentation can probe the highly dynamic outer magnetosphere and can assess both the trapped (Van Allen) radiation environment and the strongly (substorm) modulated plasma sheet conditions.

The Los Alamos National Laboratory has provided energetic particle sensors for an entire series of geostationary satellites. Each of these energetic particle instruments, consisting of several subsystems, is called the Charged Particle Analyzer (CPA) experiment. The CPA provides an environmental monitoring function for the joint Department of Energy/Department of Defense satellite of which the CPA is part and, also, the CPA provides a global assessment of magnetospheric conditions in a variety of ways (to be discussed below).

From mid-1976 to the present time, CPA instruments have collected data, in a nearly continuous fashion, on the geostationary orbit environment (although

some substantial local time coverage gaps exist early in the data set). It is the purpose of this paper to describe further the nature of the CPA measurements and then to present a summary of all available CPA energetic particle measurements made between 1976 and the current time. In particular we will describe a compilation of the geostationary data which is, in effect, an ove of the very detailed data set actually acquired and which we refer to as the Los Alamos Synoptic Data Set.

Spacecraft and Instrumentation

The data described here were acquired by the CPA instruments onboard spacecraft 1976-059, 1977-007, and 1979-053. The data from 1976-059 extend from July 1976 to the present. Similarly, the data from 1977-007 extend from early February 1977 to the present. Data from the CPA on the third satellite of this series (1979-053) has been acquired from June 1979 up to the present time. Prior to February 1977, 1976-059 was at ~ 35°W geographic longitude (at a magnetic latitude of 9°). From February 1977 onward 1976-059 was at ~ 70°W, while 1977-007 was located at ~135°W. These latter longitudinal positions correspond, respectively, to magnetic latitudes of ~11° and ~4.8°. Subsequent to June 1979, S/C 1979-053 was at ~135°W and S/C 1977-007 was at ~70°E (~8° magnetic latitude).

The CPA instruments have been described in some detail in prior published reports [Higbie et al., 1978; Baker et al., 1979a,b,c]. Each CPA consists of separate electron and proton sensor systems. The electron detectors are designated LoE (low-energy electron) and HiE (high-energy electron). LoE consists of a fan of five separate detector-collimator units at 0°, ±30°, and ±60° to the spacecraft equatorial plane. The spacecraft rotate with a 10-s period about an axis that points continually toward the center of the earth. Thus complete (over the unit sphere), continuous pitch angle measurements of

the electron distribution are made by LoE each 10-s for essentially all magnetic field orientations. Each LoE sensor-collimator unit has a geometric factor of 3.6 x $10^{-3}$ $cm^2$-sr and is sensitive to electrons of energy between 30 and 300 keV (in 6 channels). The basic CPA sampling rate is 8 ms, so that each energy channel of each sensor is sampled 40 times per 10-s spacecraft rotation (i.e. 1200 total samples per rotation).

The HiE subsystem consists of a single detector-collimator unit that is pointed radially outward in the spacecraft equatorial (0°) plane. The HiE geometric factor is 1.8 x $10^{-2}$ $cm^2$-sr and its range of sensitivity is between 0.2 MeV and ~2 MeV. Since a single collimator unit (half-angle of acceptance ~4°) is used in HiE, only a relatively narrow band of the unit sphere is sampled as the spacecraft rotates. For normal, approximately dipolar magnetic field orientations nearly all pitch angles would be sampled by HiE, but for nondipolar (taillike) magnetic field configurations often encountered near midnight at 6.6 $R_E$, very limited pitch angle sampling can result.

Both LoE and HiE have relatively thick aluminized mylar windows immediately in front of the sensitive solid state detector elements. This window eliminates contamination by sunlight, by very low energy ($\lesssim$ 10 keV) electrons, and by protons below ~ 250-300 keV. Because of this feature, LoE provides a "clean" measurement of the $\lesssim$ 300 keV electron component, free of proton or low energy pileup contributions. In the case of HiE, the measurement relies on the soft spectral nature and low relative flux ratio of the $\gtrsim$ 300 keV proton (ion) component [Baker et al., 1979c] to effect the 0.2-2.0 MeV electron measurement in the presence of background ions.

The most recent satellite in the series at geostationary orbit (1979-053) bears a further electron-measurement instrument: the spectrometer for extended electron measurements (SEE). The SEE combines thick solid state (dE/dx)

detector elements with a bismuth germanate scintillator (total E) element to provide valid electron measurements between ~2 and ~15 MeV. The measurement is made with a large geometric factor (0.15 $cm^2$-sr) and is providing a new and unprecedented look at the very high energy electron component in the outer magnetosphere.

The energetic proton measurement at 6.6 $R_E$ is made by two separate CPA particle telescope systems: LoP and HiP. LoP is a single thin (~40 μ, or ~80 μ on 1979-053) surface barrier solid state detector in front of an anticoincidence scintillator element. A sweep magnet is part of the LoP collimation system and eliminates $\lesssim$0.5 MeV electrons from entering the LoP sensors. LoP has a geometric factor of $3.9 \times 10^{-3}$ $cm^2$-sr and measures ions (which we identify as primarily protons) in the range 145 to 560 keV (10 channels). The HiP is a four-element telescope consisting of three solid state detectors encased in the fourth sensor element, a plastic anticoincidence scintillator cup. HiP also has a strong sweeping magnet to eliminate contamination by $\lesssim$ 1.0 MeV electrons. The high-energy proton telescope measures protons between 0.4 and 150 MeV in 16 quasilogarithmic differential energy channels with a geometric factor of $4.4 \times 10^{-2}$ $cm^2$-sr (~$8 \times 10^{-2}$ $cm^2$-sr for $E_p > 25$ MeV).

As in the case of the electron sensors, LoP and HiP on 1976-059 and 1977-007 (but not on 1979-053) have passive window elements to maintain light-tight operation. Like the HiE, the proton sensors consist of one collimation view direction (0°, in the spacecraft equatorial plane) so that pitch angle coverage is complete for a dipolar magnetic field orientation, but is incomplete for nondipolar (taillike) magnetic field. More thorough descriptions and illustrations of the LoP and HiP elements of the CPA (and results therefrom) are contained in several published papers [Belian et al., 1978, 1981; Baker et al., 1979c].

Data Processing

From 1976 through 1978, CPA data were processed by a set of "Phase I" analysis computer codes. The basic directional count rate arrays were read in by the programs on a rotation-by-rotation basis, particle anisotropies were calculated [Higbie and Moomey, 1977], spin-averaged count rates were formed, and 2-hour per frame microfiche plots of all quantities were generated. Thus a high time resolution (10-s) archival data set of fiche plots was produced. In addition, as the spin-averaged data set was generated, CPA data were stored to form a broader average data set (with a basic time resolution of one hour) for all particle parameters and the concatenated hour-average data tapes form the basis for the Synoptic Data Set (SDS).

Using the hour-average data tapes, a subsequent computer program sorted data for each day into eight local time bins each of 3-hour width: 0-3, 3-6,..., 21-24 LT. The sorted local time samples were then averaged together to give mean particle count rate values, etc., for each of the eight local time sectors. This local time sorting in the SDS was expected to take account of the strong local time (diurnal) variability that energetic particles exhibit, for example, due to drift-shell splitting effects.

It is well-known that interplanetary conditions substantially affect the energetic particle population at geostationary orbit [Paulikas and Blake, 1978, 1979; Baker et al., 1979b,c]. This effect, or control, appears to be primarily through the effect of solar wind bulk speed. It is further known that the solar wind parameters often undergo a recurrent and quasiperiodic variability due to long lived solar wind streams emergent from the sun [Feldman et al., 1978]. Thus, Paulikas and Blake [1979] and Baker et al. [1979b] found that long-term energetic particle flux variations could be

well-organized by plotting data in terms of solar rotation periods and we have used Carrington solar rotations to organize the Synoptic Data Set.

The 1-hour average data were used for several types of statistical analyses that form major portions of the Synoptic Data Set. These statistical studies involve, for example, assessments of probabilities that the flux of a particular energetic particle component would exceed any given flux value. These statistical studies (to be described below) are based on similar analyses performed, for example, by Paulikas et al. [1969].

From 1979 to the present the CPA data have been processed under a set of "Phase II" programs. In addition to the 10-s fiche plots, etc. which are essentially identical to the Phase I output, Phase II analysis produced a one-minute average data tape output of all computed parameters and it produced a greyscale energy-time spectrogram output. An example of the E-t spectrogram, which is extremely useful for survey purposes, will be presented below.

Examples of the High-Resolution Data Set

In order to illustrate the possible uses of the Los Alamos synchronous orbit data set, we will present figures that have been used (or are being used) in the context of various scientific studies.

Figure 1 shows an example of the greyscale energy-time spectrogram format of the Phase II output. The example shown in Figure 1 from S/C 1977-007 was generated for a substorm-event study on 8 September 1977; the CPA data have been regularly processed in this form beginning with the January 1979 data.

Each E-t spectrogram summarizes 12 hours of CPA data: electron information in the top four panels and proton (ion) information in the lower four panels. In Figure 1, data run from 0000 UT to 1200 UT (c.f. scale at the bottom of the figure) on 8 September. The top three panels in each grouping (electron or proton) show directional flux information. The top panel ($\mu$ =+1) corresponds

to field-aligned particle fluxes ($\mu = \cos\alpha$; $\alpha \lesssim 0°$). The middle panel ($\mu = 0$) corresponds to local $\alpha \sim 90°$ particles. Likewise, the third panel ($\mu = -1$) corresponds to $\alpha \lesssim 180°$ particles. Energy is shown in the ascending vertical scale in each panel (30 keV to 2 MeV for electrons and ~145 keV to 2 MeV for protons). The log of the differential particle intensity is shown by the greyscale reference bar at the left of the figure. The fourth panel from the top, and the bottom panel, summarize >30 keV electron and >145 keV proton pitch angle distributions, respectively.

As Figure 1 shows, the E-t spectrograms allow a very rapid visual scan of the temporal and spectral variations of the entire energetic particle population for a given day. Drifting "clouds" of energetic electrons and protons can be discerned throughout the period covered in the figure. Also, note that spacecraft local time (hours LT) is shown along the top of the figure. At ~0720 UT, i.e., when the spacecraft was at ~2230 LT, a sharp, intense particle injection was seen. Note also in the >30 keV electron pitch angle panel that this substorm particle injection was preceded by a very clear "cigar phase" in which $\alpha \sim 90°$ particles were strongly depleted [Baker et al., 1978]. Thus, both intensity and pitch angle variations can be readily discerned in the E-t spectrograms of the CPA data.

Since fully three-dimensional electron distribution function measurements are a prime feature of the CPA, we have developed numerous display formats to show the 3-D distributions. An example is shown in Figure 2 which is again taken from a substorm-event study based on data acquired on 28-29 December 1976. These pseudo-three-dimensional plots show the half-space with electron kinetic energy (in keV) parallel to the magnetic field ($E_{||}$) and kinetic energy perpendicular ($E_{\perp}$) to the field forming the y- and x-directions, respectively. The number of measured counts (per 8 ms sample) forms the

third, or z-direction, axis. The substorm under study in Figure 2 [Baker et al., 1981c] occurred at 0100 UT on 29 December 1976. As the sequence in Figure 2 illustrates, the $\alpha \simeq 90°$ electrons are strongly depleted relative to the 0° and 180° pitch angle particles before the substorm expansion onset. After the substorm (bottom panel), the fluxes are greatly elevated and return to the normal "trapped" distribution with perpendicularr fluxes exceeding the parallel fluxes ($j_{\perp} > j_{||}$).

The CPA data allow high temporal, as well as spatial, examination of the electron distribution function. Figure 3 shows an example of such data taken from a study of strong electron pitch angle diffusion at synchronous orbit [Baker et al., 1981a]. In the upper panel we show the (nearly constant) $\alpha \simeq 90°$ electron flux as a shaded band at $\sim 6 \times 10^7$ electrons $(cm^2\text{-}s\text{-}sr)^{-1}$. In contrast, on every spacecraft rotation the CPA sensors sample directly in the atmospheric loss cones (centered on $\alpha = 0°$ and $\alpha = 180°$). Very large and very rapid fluctuations of the loss-cone fluxes (>30 keV) can be readily discerned. This suggests that with the CPA we can begin to probe the temporal variation of equatorial energetic electron loss cone fluxes caused by resonant (whistler-mode) wave-particle interactions.

As a final example of high-resolution CPA measurements at synchronous orbit, we present high-energy proton (HiP) data in Figure 4. These data, taken from Belian et al. [1981], illustrate the pronounced temporal variations often undergone by the very energetic (>300 keV) proton component. As seen by the inset in Figure 4, a clear substorm onset occurred at 2250 UT on 14 April 1977. At this time S/C 1976-059 was at ~1800 LT and the CPA registered a two

order-of-magnitude increase in the ~500 keV differential proton flux. (Note the time structure discernible with the rapid CPA measurements.)

As shown by Belian et al. [1978, 1981] and Baker et al. [1979c], the first of the recurrent proton flux pulses such as seen in Figure 4 is due to a substorm injection of newly accelerated protons in the premidnight sector of the outer magnetosphere. This injection is quite limited both temporally and spatially such that a "pulse" of protons is seen. Subsequently (at least five times in the case of Figure 4), the pulse of protons drifts azimuthally completely around the earth. Each energy channel shows a drift-repetition time characteristic of that proton energy. These proton "drift echoes" have proven to be very useful tracers and probes of magnetosphere structure and substorm timing [Belian et al., 1978, 1981].

Long-Term Average Behavior of Particle Fluxes at 6.6 $R_E$

Just as the very high time-resolution CPA data have proven valuable in studies of the terrestrial magnetosphere, so too have longer term averages proven useful. In this section we will touch on a few of these topics.

Figure 5 illustrates a one-month run of data from two selected CPA electron energy channels (upper panel). The 200-300 keV and the 1.4-2.0 MeV daily-average fluxes for October 1976, as shown in Figure 5, exhibit a small relative increase early in the month and show a very large increase later in the month (between ~15 and 22 October). These data from a study by Baker et al. [1979b] were found to be typical of the period 1976-77. As shown by the lower panel of Figure 5, the high-energy electron increases at synchronous orbit are obviously related to increases of the solar wind bulk flow speed.

Figure 6 shows an even broader view of the time series formed by the daily-average flux values for the two selected CPA electron channels shown in Figure 5. As the reference bar above each time profile illustrates, there are

very clear periodicities seen in the electron fluxes with the highest fluxes recurring every 27 days. (In mid-1978 this periodicity tends to break down.) As seen in Figure 5, it is quite obvious to associate the 27-day periodic flux variation at 6.6 $R_E$ with the appearance at earth of high-speed solar wind streams which often recur with the 27-day periodicity of the solar rotation [c.f. Feldman et al., 1978].

Note both in Figure 5 and Figure 6 that the degree of flux modulation is much larger for the ~1.5 MeV electrons than it is for the ~0.2 MeV electrons. Also note in figure 5 that the appearance of the peak ~1.5 MeV flux at 6.6 $R_E$ is delayed by several days from the peak of $V_{sw}$ or the peak of the 0.2 MeV flux. These features of the long-term time behavior of the high-energy electron flux prompted Baker et al. [1979b] to suggest a Jovian source for the highest energy electron component in the outer terrestrial magnetosphere.

Given the intriguing questions surrounding the sources of very high-energy electrons at 6.6 $R_E$ and the causes of the variability, it was of great interest to measure even higher in energy. Questions of concern included: How high in energy does the "magnetospheric" electron component go? Is the >1 MeV component more strongly modulated than the <1 MeV electron population? The SEE sensor, giving good measurements in the 2-15 Mev range, has now permitted some initial answers to such questions.

Figure 7 summarizes electron differential energy spectra acquired by the HIE and SEE sensors onboard SMS 1979-052 between 10 June and 20 June 1980. The spectra are in a "stacked-spectrum" format and are averages of the fluxes measured near local noon on each day. We find that even on June 10 and June 11, the 2 MeV electron flux greatly exceeds the NASA AE-8 model environment; from June 12 to 20 the very high energy electrons (> to >10 MeV) increase in intensity by at least 2-3 orders of magnitude. This June 1980 period is the

largest "SEE" event we have found to date, but SEE measurements also reveal a rather frequent occurrence of very high-energy electron flux increases. Thus, the SEE sensor is providing a new perspective on the outer radiation zone and may allow us to unravel the mystery of where the highest energy electrons come from.

The Synoptic Data Plots

Prompted by long-term results such as those seen in Figures 5-7, we compiled the Los Alamos Synoptic Data Set [Baker et al., 1981b]. The SDS plots are divided into two parts: one for S/C 1976-059 and one for S/C 1977-007. As discussed above, the periods of data coverage from the two spacecraft largely overlap and instrumentation is essentially identical. Therefore, differences between the measurements of the CPA's aboard the two satellites made at the same time must be primarily due either to magnetic latitude effects which can be quite large [c.f. Baker et al., 1981], or else to local time effects.

For each solar rotation, three pages of data are given. As illustrated by Figure 8 (for Carrington Rotation #1956) the first type of plot in each solar rotation series illustrates pseudo-three-dimensional stacked spectrum plots. We have averaged all local time data together for electrons and ions separately and have calculated the daily-average particle differential energy spectrum. Then, for each day of the solar rotation we plot the logarithm (base 10) of the electrons or protons $(cm^2\text{-}s\text{-}sr\text{-}keV)^{-1}$ versus the logarithm of the particle kinetic energy (in keV). The third (or perspective) dimension of each plot is solar rotation day number (from 1 to 27) running to the right.

The upper part of each daily spectrum page illustrates the variation in electron distribution functions between 50 keV and 2000 keV. In order to aid in the 3-D representation of the spectral variation, several dashed lines are

added to each plot. These include four dashed lines running entirely across the solar rotation period connecting the spectra at four specific energy channel points. These dashed lines are intended to help the user visualize the "spectral surface" that the CPA determines for each solar rotation period.

The lower part of the daily spectrum page illustrates the variation in proton (ion) distribution functions above 145 keV. As may be noted for C. R. # 1955 data, proton fluxes typically reach a background level of $\sim 10^{-2}$ $(cm^2\text{-}s\text{-}sr\text{-}keV)^{-1}$ at $F_p \sim 1000$ keV. Thus, although the CPA makes proton measurements up to 150 MeV we typically show the proton spectrum only up to ~20 MeV. During solar flares, or other periods of exceptionally large high-energy proton flux, we extend the plotted proton energy range appropriately.

Although not shown here, in the SDS we also present two-dimensional flux profile plots similar to Figure 5. The Synoptic plots of this type, however, show the flux profiles broken down according to Carrington rotation number and also show separate plots for 6 electron channels and 10 proton channels averaged over 3-hour local time groupings as described previously.

In essence, the stacked-spectrum plots give an overview of the spectral and temporal variability of the energetic particle populations for any given solar rotation period. These somewhat qualitative results are complemented by the more detailed local-time-sorted data provided in the two-dimensional flux-time plots. Beyond this level of detail, e.g., for evaluation of very detailed particle variation features, pitch angle effects, and other high-frequency phenomena, one must use the Synoptic Data Set as a guide and return to the fundamental archival high-resolution data base for detailed analysis.

The last part of the SDS deals with very broad statistical analyses of the CPA data base. Here the one-hour data tapes were used as input, and

statistical evaluations were made over periods long compared to a solar rotation. The flux probability plots, such as that shown in Figure 9, summarize the chances that, at any given energy, the integral particle flux ($cm^{-2}$-$s^{-1}$-$sr^{-1}$) will exceed a particular value. These plots are expected to be of interest for instrument design, spacecraft engineering, and environmental monitoring. They may be of especial interest to operators looking at energetic particle data in real time by providing a baseline for the interpretation or prediction of rapid variations in particle fluxes.

Applications and Scientific Uses of the Los Alamos Data Set

The Synoptic Data Set is a broad compilation of information concerning the radiation environment at geostationary orbit. As discussed in the Introduction, the geostationary orbit is useful both to the applications community and to the scientific community.

By 'applications community' we mean those persons and organizations who use the atmosphere and/or outer space for commercial, engineering, or military purposes. This community often needs to know the geomagnetic and magnetospheric environmental conditions in order to better carry out its tasks, e.g., spacecraft design, communication, or satellite operation.

Within the domain of the applications community, we believe that the statistical studies such as presented here would be particularly useful. Our statistical results clearly indicate what flux levels of energetic particles may be expected to be encountered at geostationary orbit. The probability levels assigned to various flux levels of the different particle components should allow better assessment of design criteria for future geostationary satellite missions, as an example.

We expect that the SDS can also be useful in evaluating events of interest to the applications community well-after these events have occurred. For example, spacecraft operational anomalies or atmospheric disturbances (affecting radio propagation) can at times be interpreted in terms of energetic particle enhancements in the outer magnetosphere. The data presented here (and those data which continue to be collected by CPAs on orbit) are readily available for use by the applications community for their needs. Data are also available from these satellites in real time for qualified users in the applications community for environmental monitoring purposes.

Within the scientific community, a major goal is to come to a better understanding of magnetospheric structure and dynamics. Relevant questions include where energetic plasma particles originate, how the particles are subseqently transported, and how they are eventually lost (e.g., precipitated into the terrestrial atmosphere). Long-term overviews of the time variations of energetic particle fluxes such as given by the SDS can lead to a better predictive capability in the future [c.f. Paulikas and Blake, 1978, 1979; Higbie et al., 1979; Baker et al., 1979b,c; West et al., 1979].

A major point of presenting this paper at this Symposium is that the International Magnetospheric Study (IMS) was organized to gain an improved understanding of the terrestrial magnetosphere. The observational phase of the IMS extended from 1977 through 1979. Therefore, the Los Alamos Synchronous Orbit Data Set as presented here overlaps completely with the IMS observational period and provides a very relevant data base for IMS comparative studies. We strongly encourage the scientific community to use the Los Alamos data set as a basis for evaluating general energetic particle conditions in the magnetosphere and we look forward to cooperative studies of magnetospheric processes with other interested researchers.

Acknowledgments

We thank W. Aiello for electronic development of the CPA, and E. Tech, M. Halbig, J. Payne, R. Robinson, and S. Kedge for data analysis support. We also thank J. B. Blake (Aerospace) and D. T. Young (University of Bern) for many useful discussions. This work was done under the auspices of the U.S. Department of Energy.

References

Baker, D. N., P. R. Higbie, E. W. Hones, Jr., and R. D. Belian, High-resolution energetic particle measurements at 6.6 RE, 3, Low-Energy electron anisotropies and short-term substorm predictions, J. Geophys. Res., 83, 4863, 1978.

Baker, D. N., P. Stauning, E. W.Hones, Jr., P. R. Higbie, and R. D. Belian, Strong electron pitch angle diffusion observed at geostationary orbit, Geophys. Res. Letters, 6, 205, 1979a.

Baker, D. N., P. R. Higbie, R. D. Belian, and E. W. Hones, Jr., Do Jovian electrons influence the terrestrial outer radiation zone?, Geophys. Res. Letters, 6, 531, 1979b.

Baker, D. N., R. D. Belian, P. R. Higbie, and E. W. Hones, Jr., High Energy magnetospheric protons and their dependence on geomagnetic and interplanetary conditions, J. Geophys. Res., 84, 7138, 1979c.

Baker, D. N., P.R. Higbie, and R. D. Belian, Multispacecraft observations of energetic flux pulsations at 6.6 $R_E$, J. Geophys. Res., 85, 6709, 1980.

Baker, D. N., P. Stauning, E. W. Hones, Jr , P. R. Higbie, and R. D. Belian, Near-equatorial, high-resolution measurements of electron precipitation at L ~ 6.6, J. Geophys. Res., 86, A4, 1981a.

Baker, D. N., P. R. Higbie, R. D. Belian, W. P. Aiello, E. W. Hones, Jr., F. L. Tech, M. F. Halbig, J. B. Payne, R. Robinson, and S. Kedge, The Los Alamos geostationary orbit synoptic data set : A compilation of energetic particle data, Los Alamos National Laboratory report, June, 1981b.

Baker, D. N., E. W. Hones, Jr., P. R. Higbie, R. D. Belian, and P. Stauning, Global Properties of the magnetosphere during a substorm growth phase: A case study, J. Geophys. Res., submitted for publication, 1981c.

Belian, R. D., D. N. Baker, P. R. Higbie, and E. W. Hones, Jr., High-resolution energetic particle measurements at 6.6 $R_E$, 2, High-energy proton drift echoes, J. Geophys. Res., 83, 4857, 1978.

Belian, R. D., D. N. Baker, E. W. Hones, Jr., P.R. Higbie, S. J. Bame, and J. R. Asbridge, Timing of energetic proton enhancements relative to magnetospheric substorm activity and its implication for substorm theories, J. Geophys. Res., 86, 1415, 1981.

Feldman, W. C., J. R. Asbridge, S. J. Bame, and J. T. Gosling, Long-term variations of selected solar wind properties: IMP 6, 7, and 8 results, J. Geophys. Res., 83, 2177, 1978.

Higbie, P. R., and W. R. Mooney, Pitch angle measurements from satellites using particle telescopes with multiple view directions, Nucl. Instrum. and Methods, 146, 439, 1977.

Higbie, P. R., R. D. Belian, and D. N. Baker, High-resolution particle measurements at 6.6 $R_E$, 1, Electron micropulsations, J Geophys. Res. 83, 4851, 1978.

Higbie, P. R., D. N. Baker, V. Domingo, W. L. Imhof, R. L. McPherron, W. N. Spjeldvik, D. J. Williams, J. R. Burrows, and M. Hayakawa, Short term magnetospheric particle variations (1 min < T < 1 day), Solar-Terrestrial Predictions Proceedings, Vol. 2, (R. F. Donnelly, Ed.), p. 434, 1979.

Paulikas, G. A., J.B. Blake, and J. A. Palmer, Energetic electrons at synchronous altitude: A compilation of data, Aerospace Corp., Rep. No. TR-0066(5260-20)-4, November, 1969.

Paulikas, G. A., and J. B. Blake, Energetic electrons at synchronous altitude 1965-1977, Aerospace Corp., Rep. No., TR-0078(3260-05), March, 1978.

Paulikas, G. A., and J. B. Blake, Effects of the solar wind on magnetospheric dynamics: Energetic electrons at the synchronous orbit, Quantitative

Modeling of Magnetospheric Processes, 21, Geophys. Monograph Series (W. P. Olson, Ed.), p. 180, 1979.

West, H. I., Jr., R. M. Buck, G. Davidson, Study of energetic electrons in the outer radiation-belt regions using data obtained by the LLL spectrometer on OGO-5 in 1968, Lawrence Livermore Rep. UCRL-52807, July, 1979.

Figure Captions

Fig. 1. A greyscale energy-time spectrogram summarizing CPA data from S/C 1977-007 on 8 September 1977.

Fig. 2. Three-dimensional representations of the CPA electron count rate versus perpendicular ($E_{\perp}$) and parallel ($E_{||}$) kinetic energy (keV) for 2359, 0031, and 0156 UT on 28-29 December 1976

Fig. 3. High temporal resolution measurements of the >30 keV electron fluxes at synchronous orbit on 18 September 1976. The trapped ($\alpha \gtrsim 90°$) and loss-cone ($\alpha \lesssim 0°, 180°$) fluxes are shown. The bottom panel shows simultaneous Narssarssuaq riometer data (i.e., data indicative of electron precipitation at the foot of the field line passing near S/C 1976-059 at 6.6 $R_E$).

Fig. 4. High-energy proton drift-echo data measured by the CPA aonboard S/C 1976-059 late on 14 April 1977.

Fig. 5. Daily average electron fluxes (upper panel) measured by the CPA during October 1976 compared to the concurrently measured solar wind bulk speed (lower panel). A clear correlation between synchronous orbit particle fluxes and $V_{sw}$ is seen.

Fig. 6. A long-term plot of CPA daily-average electron fluxes for portions of 1977 and 1978. A clear 27-day periodicity in the fluxes is seen.

Fig. 7. Combined CPA (HiE) and SEE electron data for 10-20 June 1980. The stacked-spectrum format shows the large rise in the >2000 keV electron fluxes after 17 June and demonstrates the very hard energy spectrum observed out to >10000 keV.

Fig. 8. An example of the Synoptic Data Set stacked-spectrum plots (as described in the text) for Carrington solar rotation 1955.

Fig. 9. Flux probability plots for July through December 1976. The data are for S/C 1976-059 and the upper panel shows electron data with integral thresholds (from right to left) of $E_e$ >30, >65, >140, >200, >430, and >930 keV. The lower panel summarizes flux probabilities for proton integral thresholds (right to left) of $E_p$ >145, >175, >215, >290, >400, >500, >800, and >1000 keV.

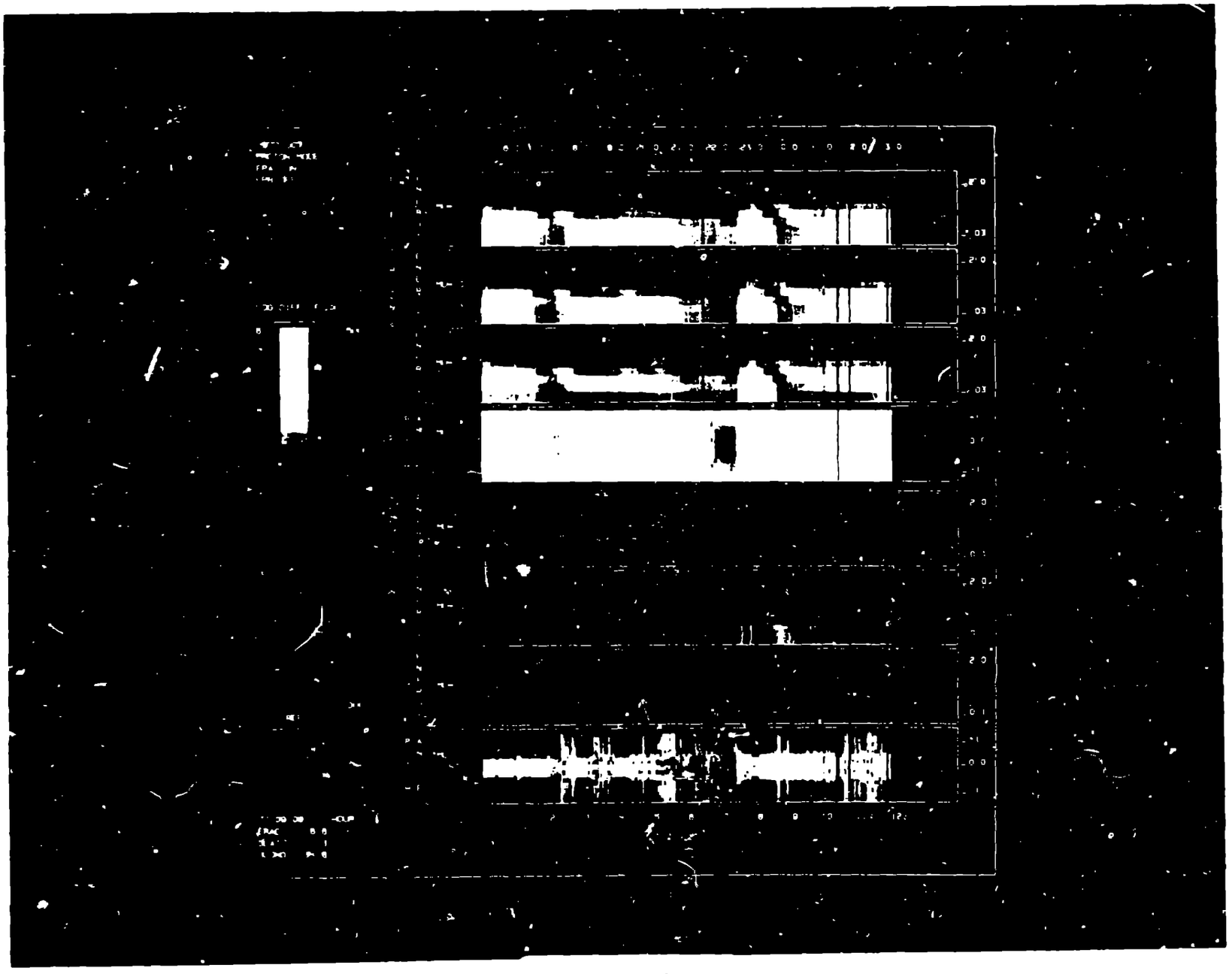

Figure 1

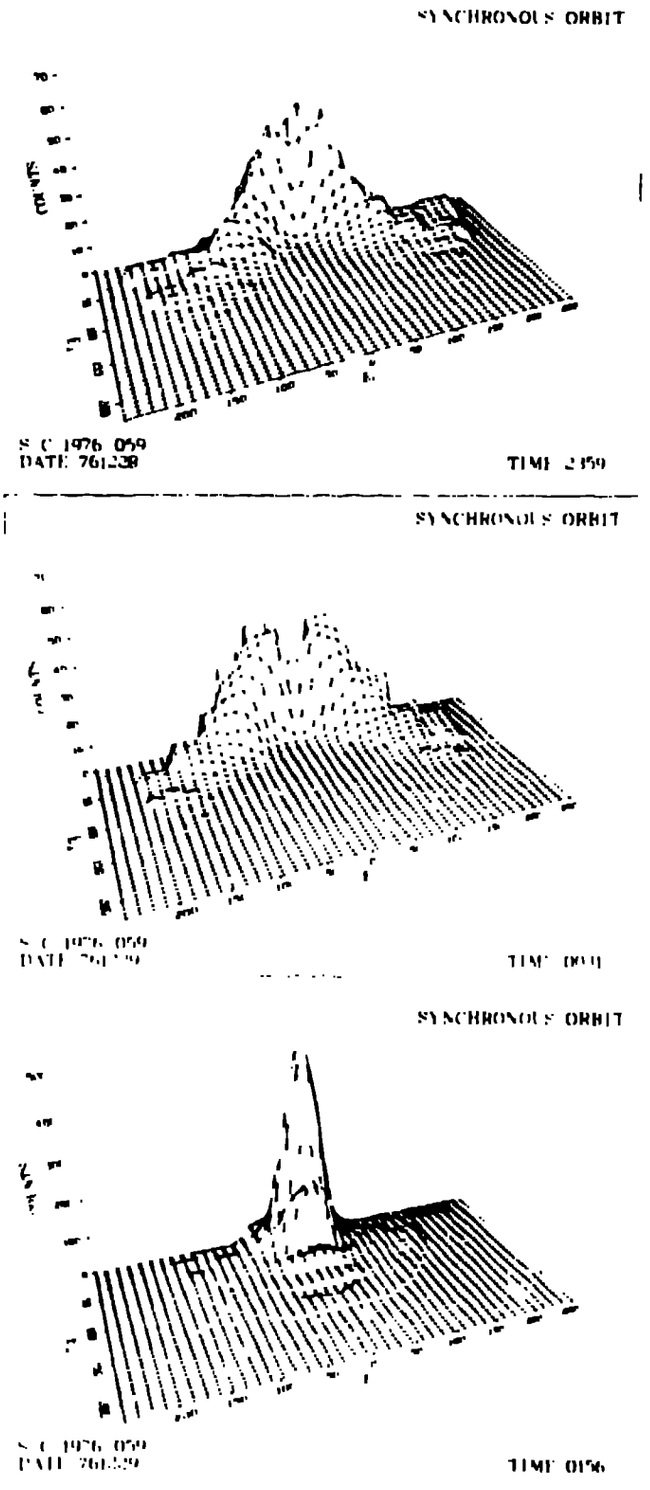
SYNCHRONOUS ORBIT
S/C 1976 059
DATE 761238
TIME 2359
SYNCHRONOUS ORBIT
TIME 0001
SYNCHRONOUS ORBIT
TIME 0156

Fig. 2

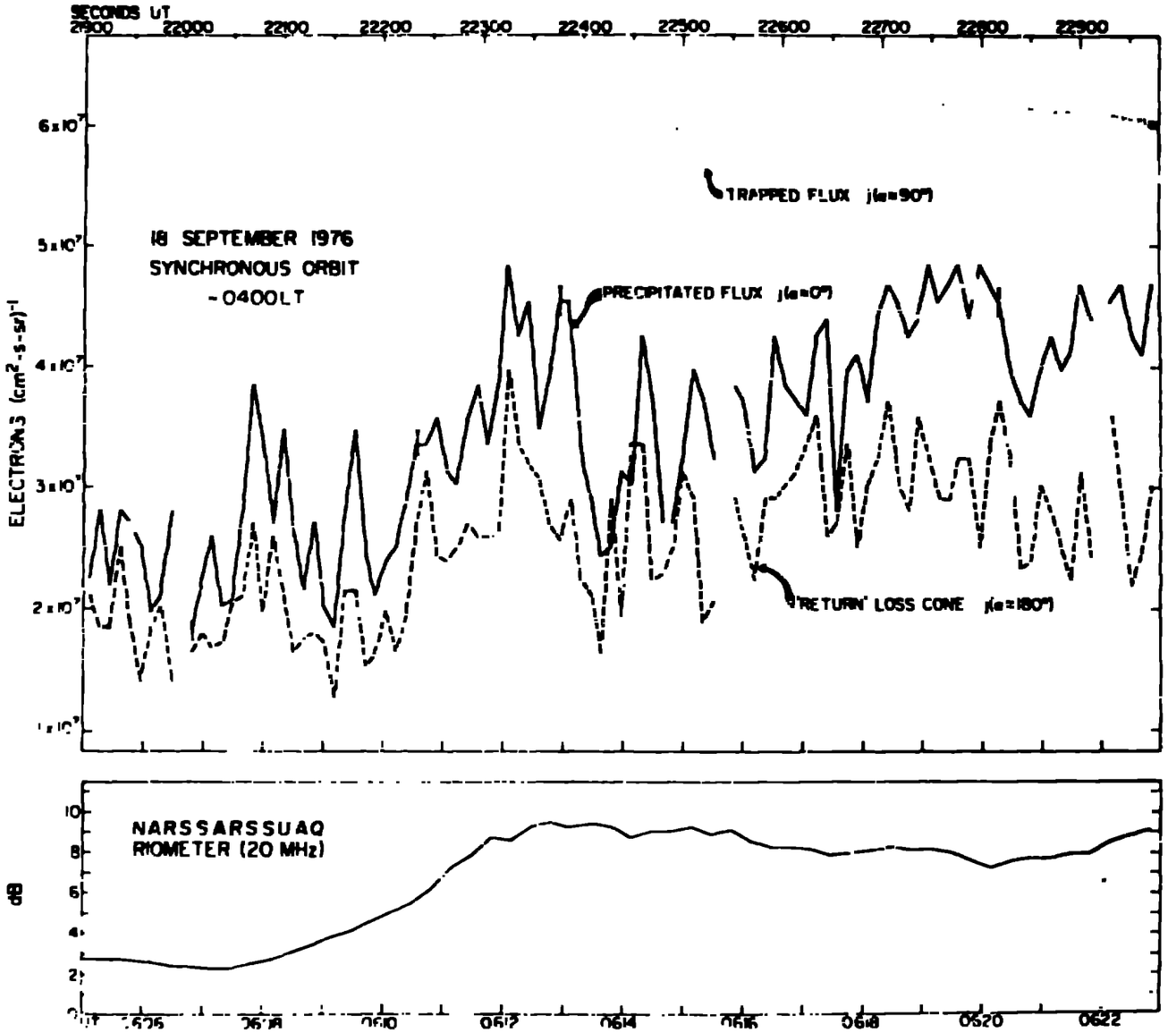
SECONDS UT
21900
22000
22100
22200
22300
22400
22500
22600
22700
22800
22900
6x10⁷
5x10⁷
4x10⁷
3x10⁷
2x10⁷
ELECTRONS (cm²-s-sr)⁻¹
18 SEPTEMBER 1976
SYNCHRONOUS ORBIT
-0400LT
TRAPPED FLUX j(α=90°)
PRECIPITATED FLUX j(α=0°)
'RETURN' LOSS CONE j(α=180°)
NARSSARSSUAQ
RIOMETER (20 MHz)
dB
10
8
6
4
2
0
0605
0608
0610
0612
0614
0616
0618
0620
0622

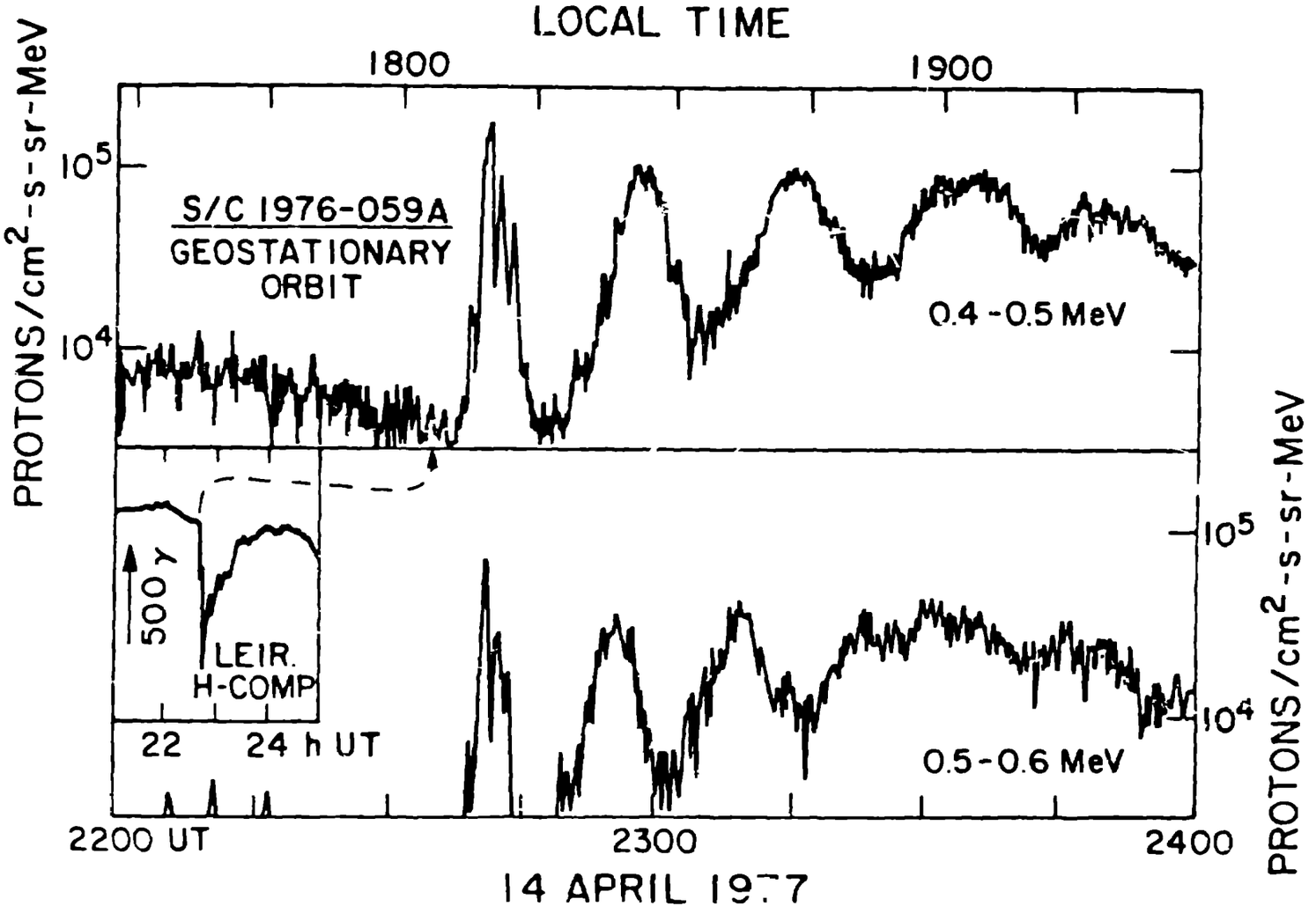
LOCAL TIME
1800
1900
PROTONS/cm²-s-sr-MeV
10⁵
10⁴
S/C 1976-059A
GEOSTATIONARY
ORBIT
0.4 - 0.5 MeV
500 γ
LEIR.
H-COMP
22
24 h UT
0.5 - 0.6 MeV
2200 UT
2300
2400
14 APRIL 1977

Fig. 1

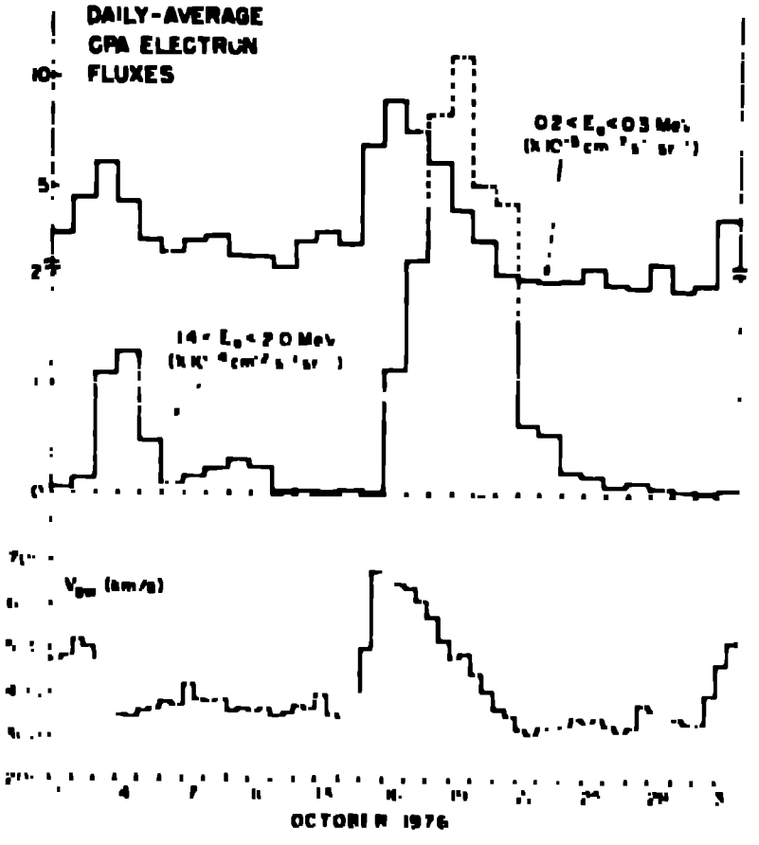
DAILY-AVERAGE
GPA ELECTRON
FLUXES
10
5
2
0.2 < E_e < 0.3 MeV
1.4 < E_e < 2.0 MeV
V_sw (km/s)
OCTOBER 1976

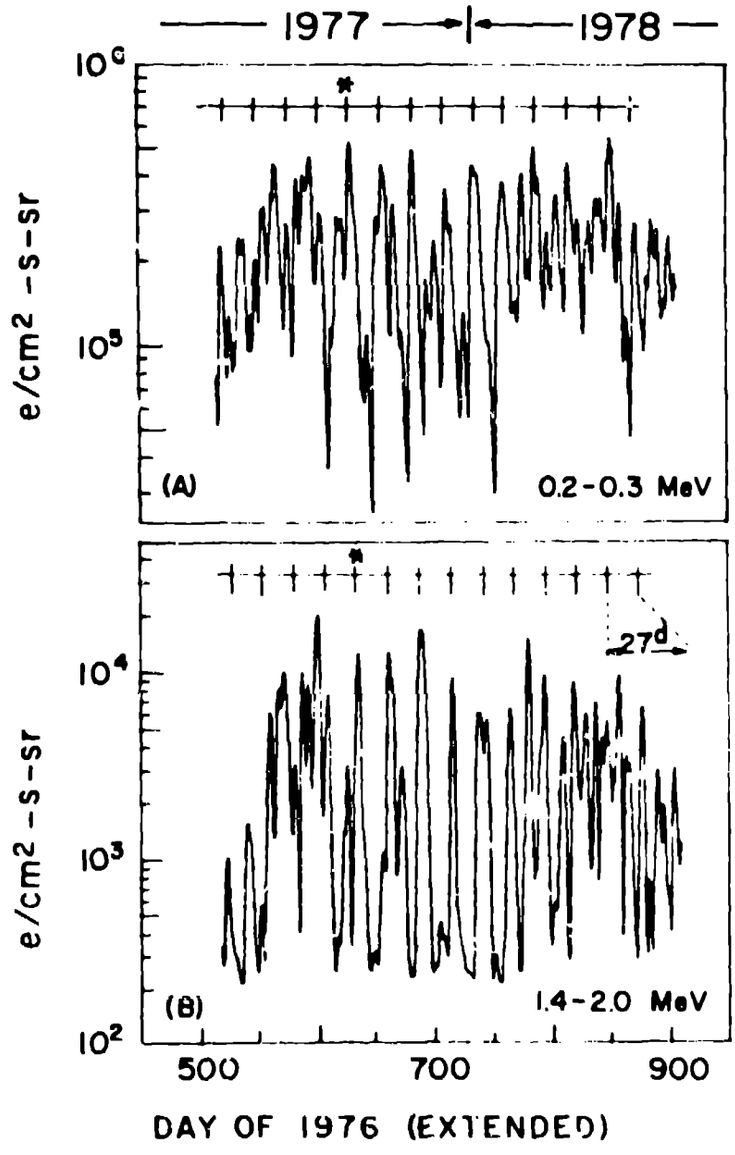
1977
1978
$10^6$
$10^5$
e/cm2 -s-sr
(A)
0.2-0.3 MeV
$10^4$
$10^3$
$10^2$
27d
(B)
1.4-2.0 MeV
500
700
900
DAY OF 1976 (EXTENDED)

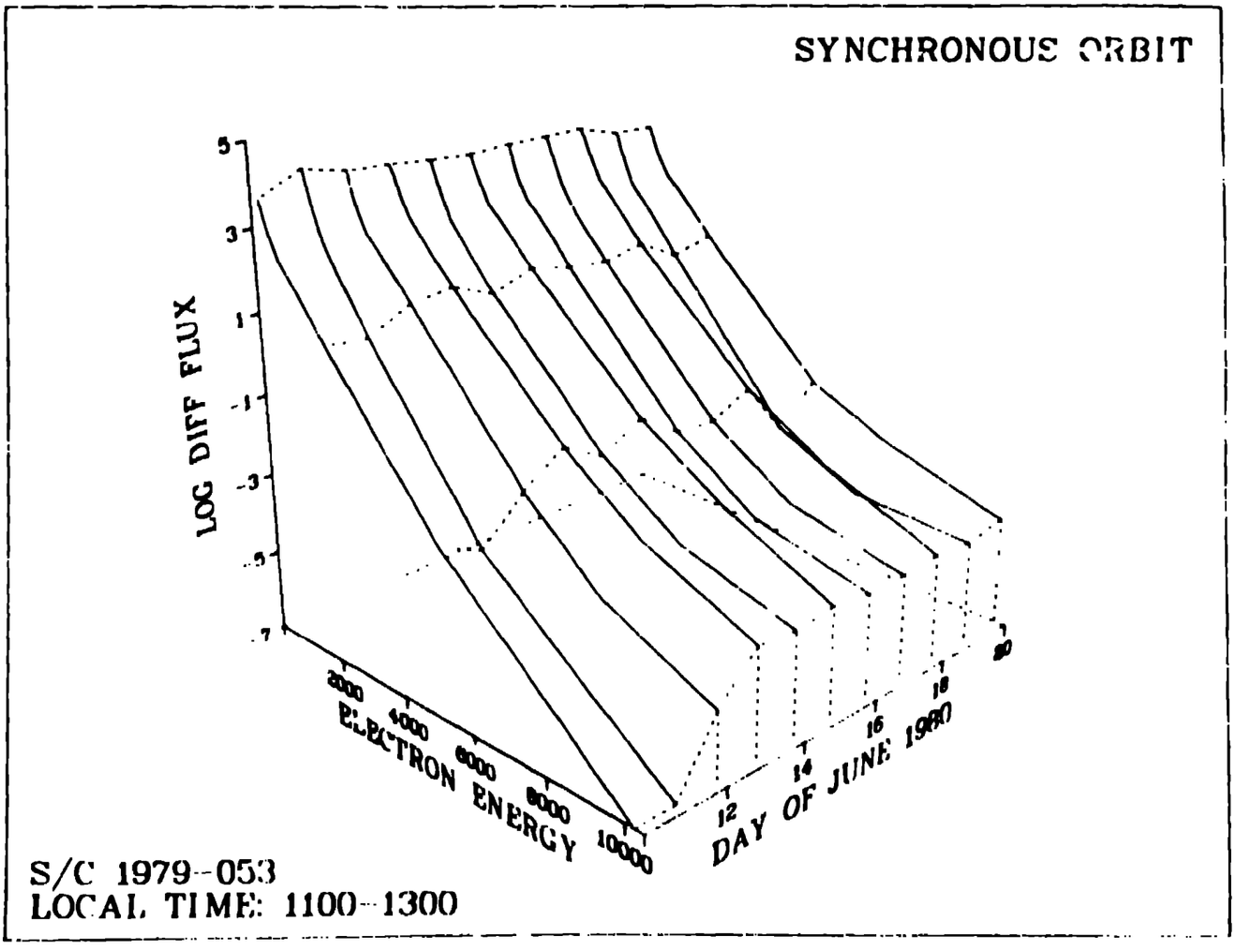
SYNCHRONOUS ORBIT
LOG DIFF FLUX
5
3
1
-1
-3
-5
-7
2000
4000
6000
8000
10000
ELECTRON ENERGY
12
14
16
18
DAY OF JUNE 1980
S/C 1979-053
LOCAL TIME: 1100-1300

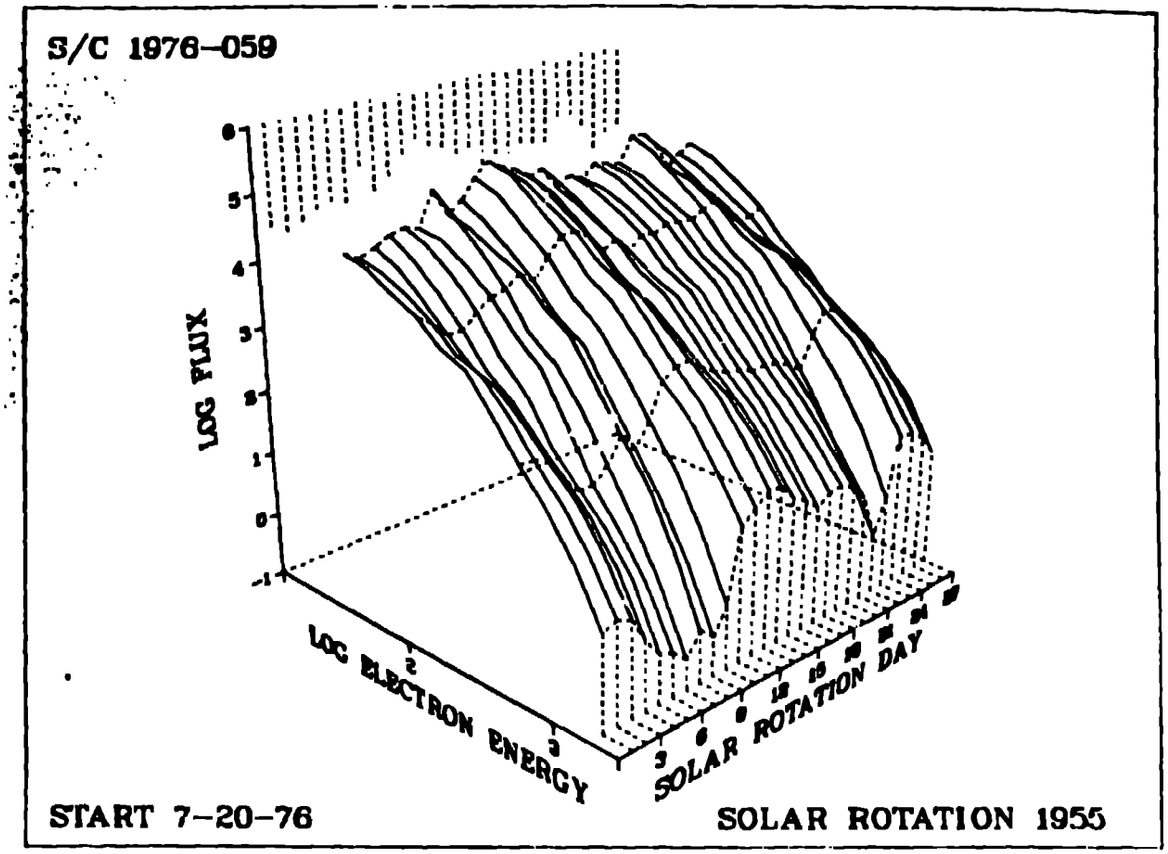
S/C 1976-059
LOG FLUX
LOG ELECTRON ENERGY
SOLAR ROTATION DAY
START 7-20-76
SOLAR ROTATION 1955

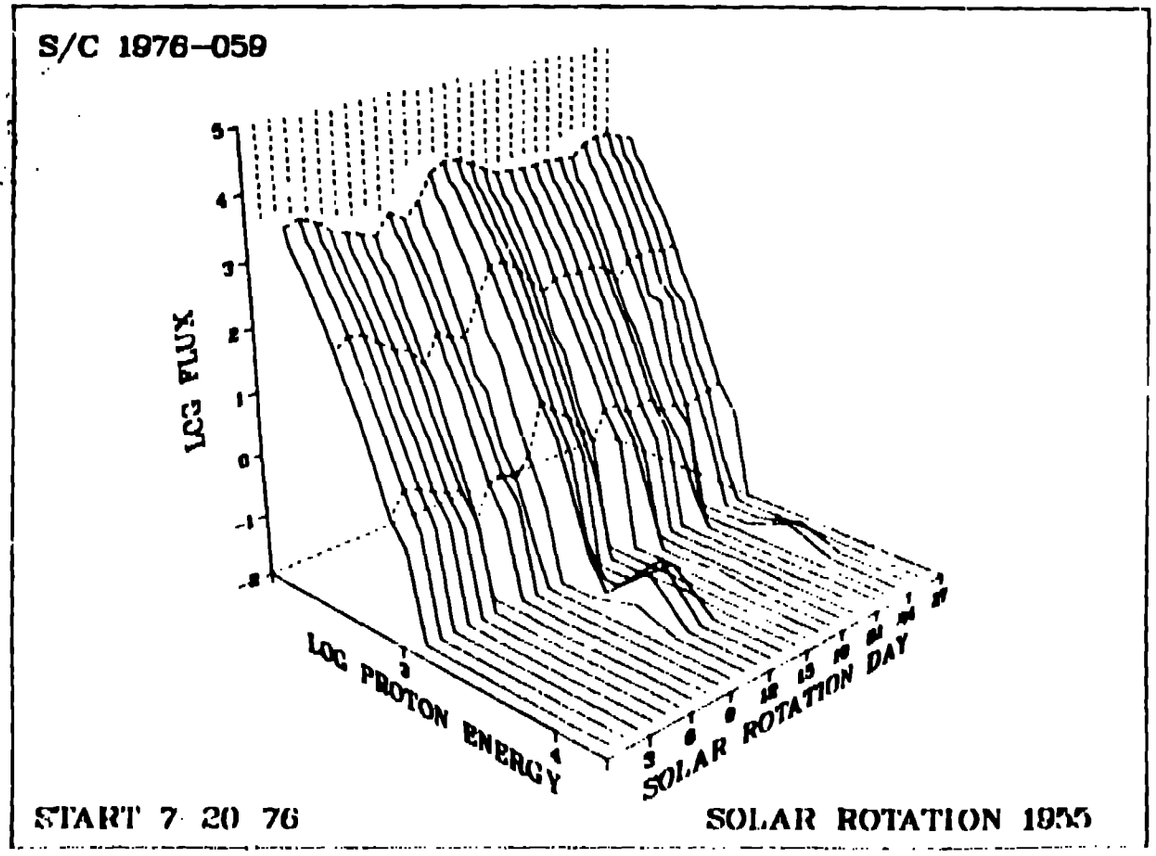
S/C 1976-059
LOG FLUX
LOG PROTON ENERGY
SOLAR ROTATION DAY
START 7 20 76
SOLAR ROTATION 1955

Fig. 8

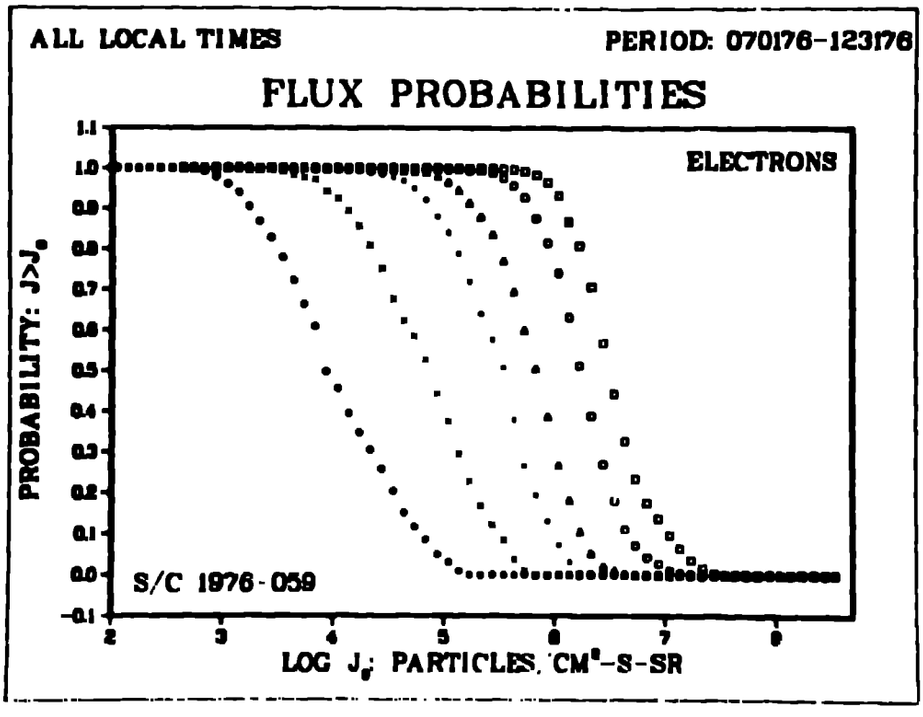
ALL LOCAL TIMES
PERIOD: 070176-123176
FLUX PROBABILITIES
ELECTRONS
PROBABILITY: J>J$_0$
S/C 1976-059
LOG J$_0$: PARTICLES/CM$^2$-S-SR

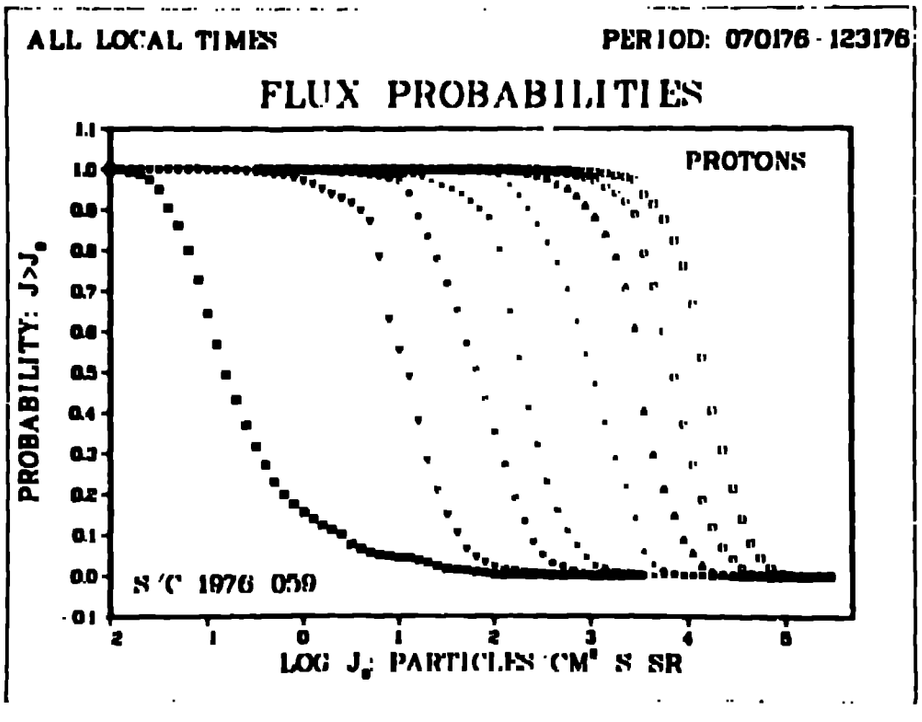
ALL LOCAL TIMES
PERIOD: 070176-123176
FLUX PROBABILITIES
PROTONS
PROBABILITY: J>J$_0$
S/C 1976-059
LOG J$_0$: PARTICLES/CM$^2$-S-SR